In situ measurement of atmospheric CO2 at the four WMO/GAW stations in China

S. Fang, L. Zhou, P. Tans, Philippe Ciais, M. Steinbacher, L. Xu, T. Luan

Atmos. Chem. Phys., 14, 2541–2554, 2014
www.atmos-chem-phys.net/14/2541/2014/
doi:10.5194/acp-14-2541-2014

Atmospheric Chemistry and Physics Open Access

In situ measurement of atmospheric CO_2 at the four WMO/GAW stations in China

S. X. Fang[1], L. X. Zhou[1], P. P. Tans[2], P. Ciais[3], M. Steinbacher[4], L. Xu[1], and T. Luan[1]

[1]Chinese Academy of Meteorological Sciences (CAMS), China Meteorological Administration (CMA), Beijing, China
[2]Earth System Research Laboratory (ESRL), National Oceanic and Atmospheric Administration (NOAA), Boulder, CO, USA
[3]Laboratory for the Science of Climate and the Environment (LSCE), Paris, France
[4]Empa, Swiss Federal Laboratories for Materials Science and Technology, Laboratory for Air Pollution/Environmental Technology, Duebendorf, Switzerland

Correspondence to: L. X. Zhou (zhoulx@cams.cma.gov.cn)

Received: 31 August 2013 – Published in Atmos. Chem. Phys. Discuss.: 21 October 2013
Revised: 25 January 2014 – Accepted: 6 February 2014 – Published: 12 March 2014

Abstract. Atmospheric carbon dioxide (CO_2) mole fractions were continuously measured from January 2009 to December 2011 at four atmospheric observatories in China using cavity ring-down spectroscopy instruments. The stations are Lin'an (LAN), Longfengshan (LFS), Shangdianzi (SDZ), and Waliguan (WLG), which are regional (LAN, LFS, SDZ) or global (WLG) measurement stations of the World Meteorological Organization's Global Atmosphere Watch program (WMO/GAW). LAN is located near the megacity of Shanghai, in China's economically most developed region. LFS is in a forest and rice production area, close to the city of Harbin in northeastern China. SDZ is located 150 km northeast of Beijing. WLG, hosting the longest record of measured CO_2 mole fractions in China, is a high-altitude site in northwestern China recording background CO_2 concentration. The CO_2 growth rates are 3.7 ± 1.2 ppm yr^{-1} for LAN, 2.7 ± 0.8 ppm yr^{-1} for LFS, 3.5 ± 1.6 ppm yr^{-1} for SDZ, and 2.2 ± 0.8 ppm yr^{-1} (1σ) for WLG during the period of 2009 to 2011. The highest annual mean CO_2 mole fraction of 404.2 ± 3.9 ppm was observed at LAN in 2011. A comprehensive analysis of CO_2 variations, their diurnal and seasonal cycles as well as the analysis of the influence of local sources on the CO_2 mole fractions allows a characterization of the sampling sites and of the key processes driving the CO_2 mole fractions. These data form a basis to improve our understanding of atmospheric CO_2 variations in China and the underlying fluxes using atmospheric inversion models.

1 Introduction

Carbon dioxide (CO_2) represents the most important contribution to increased radiative forcing (IPCC, 2007). The increase of atmospheric CO_2 of ~ 110 ppm above preindustrial levels has been unequivocally attributed to human emissions (GLOBALVIEW-CO_2, 2012; Keeling, 1993). These emissions are mainly coming from fossil fuel burning and land-use changes (Houghton, 2003; Peters et al., 2012). The oceans and terrestrial ecosystems act as sinks for atmospheric CO_2 and absorb approximately half of the anthropogenic emissions (Ballantyne et al., 2012). To enhance our understanding of the carbon cycle, it is crucial to quantify atmospheric CO_2 variations as they are influenced by regional fluxes (Peters et al., 2007; Tans et al., 1990). For this purpose, 55 years ago, long-term measurements of atmospheric CO_2 concentration began at Mauna Loa, Hawaii (Keeling et al., 1976; Keeling, 2008). So far, there are more than 150 sites worldwide where greenhouse gas concentrations are measured (Artuso et al., 2009; Dlugokencky et al., 1995; Necki et al., 2003; Sirignano et al., 2010; Tans et al., 1990; WMO, 2012). Studies show that the current global CO_2 observation network can at best constrain emissions at continental scales, and that tropical regions remain unconstrained because observations in that region are too sparse (Chevallier et al., 2011; Thompson et al., 2009). Regional networks with ongoing CO_2 observations measure gradients between stations, which can be used to retrieve information on regional emissions and sinks. At present, relatively dense networks exist

over North America and western Europe, which allow us to constrain regional fluxes using inverse models (e.g., Broquet et al., 2013; Gourdji et al., 2012). But northeastern Asia, a region of fast economic growth with high emissions, is not adequately sampled, and global inversion results give divergent results for its CO_2 budget (e.g., Peylin et al., 2013; Sirignano et al., 2010).

With the rapid development of its economy, China has become the number one fossil fuel CO_2 emitter in 2006 and emitted 1.8 Pg C in 2011 (LeQuéré et al, 2013; Marland, 2012). The emissions of China deduced from energy statistics are uncertain, and could be higher than currently reported by up to 0.38 g C yr^{-1} (Guan et al., 2012). Peters et al. (2011) also reported that more than half of the growth in global CO_2 emissions from 1990 to 2008 took place in China. China is a late starter of atmospheric greenhouse gas observations. In the past years, there have been lots of short-term CO_2 measurement campaigns and research programs. Most of these focused on emissions from agricultural sources or urban areas (Fu et al., 2009; Lei and Yang, 2010; Liu et al., 2009; Tang et al., 2006; Xing et al., 2005). Long-term atmospheric CO_2 observations in China have been relatively sparse. The China Meteorological Administration (CMA) has been responsible for background greenhouse gas measurements. The first station installed in China is Mt. Waliguan (WLG) in Qinghai province, at 3816 m a.s.l. Since May 1991, CMA has collected weekly air samples in glass flasks. These samples were shipped to the National Oceanic and Atmospheric Administration (NOAA) Earth System Research Laboratory (ESRL) in Boulder, Colorado, United States, and analyzed for a suite of greenhouse gases. In 1994, the station was established as a global World Meteorological Organization (WMO) Global Atmosphere Watch (GAW) measurement site, and was equipped to measure CO_2 mole fractions by means of a LI-COR nondispersive infrared (NDIR) analyzer. This instrument produced nearly 14 years of high-quality data, which is the longest continuous atmospheric CO_2 record in China (Zhou et al., 2003, 2005, 2006). In 2009, the aging instrument was replaced by a cavity ring-down spectroscopy (CRDS) analyzer (G1301, Picarro Inc.). Three greenhouse gases measurement stations were established as regional WMO/GAW sites at Lin'an (LAN) in Zhejiang province (near Shanghai), Longfengshan (LFS) in Heilongjiang province (near Harbin, in the northeast of China), and Shangdianzi (SDZ) near Beijing. The information of the station is accessible at http://gaw.empa.ch/gawsis/default.asp. Initially, those were automatic weather stations only, and in situ CO_2/CH_4 measurement systems began in 2009 using CRDS instruments (G1301). In the previous study, we presented and analyzed the first 3 years CH_4 mole fractions observed at LAN, LFS, and WLG (Fang et al., 2013). Similarly, here we study the observed CO_2 mole fractions at the four stations.

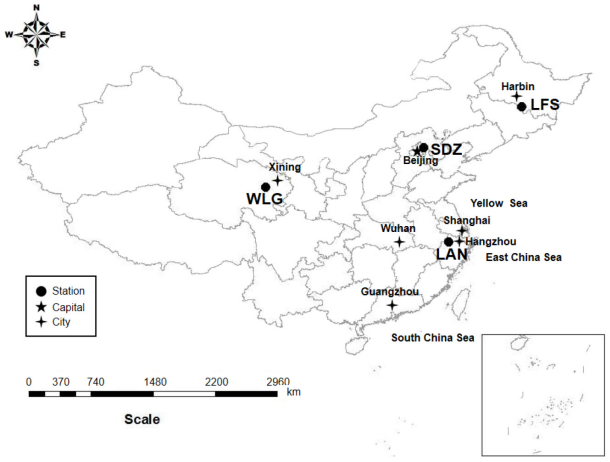

Fig. 1. Locations of the four Chinese WMO/GAW stations.

2 Experimental

2.1 Sampling sites

Locations of Lin'an (LAN), Longfengshan (LFS), Shangdianzi (SDZ), and Mt. Waliguan (WLG) are shown in Fig. 1. Information of the four stations is listed in Table 1. LAN is located at the center of the Yangtze Delta area, China, and is about 50 km from Hangzhou (the capital of Zhejiang province) and 150 km from Shanghai (the largest economic center in China). This station is approximately 6 km northeast of the town of Lin'an, which has a population of $\sim$ 100 000. North of the LAN station (1.4 km away) is a small factory where charcoal is manufactured from bamboo wood. The station is built on the top of a small hill and is surrounded by a few pieces of paddy rice field.

LFS is 175 km southeast of Harbin city. Wuchang, the nearest city, has $\sim$ 200 000 inhabitants and is 40 km to the northwest of the site. The station is located on the northwest edge of the Longfengshan water reservoir, which has an area of 20 km^2. The reservoir's dam is located 100 m to the north of LFS. Right beyond the dam to the north, there is a small area of paddy rice field and several small villages ($\sim$ 100 inhabitants). The station is located in a forest park with mainly pine trees.

SDZ is located at 150 km northeast of Beijing. The observatory is built on a mountainside (with the highest peak to the north). There is a small village ($\sim$ 300 inhabitants) at about 0.8 km to the south of the station. A railway used by diesel-driven trains runs from southwest to northeast, $\sim$ 0.6 km away from the station. The local vegetation is mainly shrubs and corn.

WLG is situated in western China at 3816 m a.s.l., and is far from industrial and populated centers. Measurements from WLG provide essential information on sources and sinks over the Eurasian continent (Zhou et al., 2004, 2005).

Table 1. Descriptions of the four WMO/GAW stations in China.

Station	Station ID	Longitude	Latitude	Altitude (m a.s.l.)	Intake height (m a.g.l.)	Representation area	Vegetation canopy
Lin'an	LAN	119.72° E	30.3° N	138.6	10, 50	Yangtze Delta economic zone	Paddy, wheat field, shrub
Longfengshan	LFS	127.6° E	44.73° N	330.5	10, 80	Northeastern Plain	Paddy, forest
Shangdianzi	SDZ	117.12° E	40.65° N	293.3	10, 80	North China Plain	Shrub, corn
Mt. Waliguan	WLG	100.06° E	36.12° N	3816	10, 80	Northeastern part of the Tibetan Plateau	Prairie sandbank

At SDZ, LAN, and LFS, the sampling inlets were initially fixed on the top of wind poles (10 m a.g.l.). Near each sampling inlet, a wind direction and speed sensor were also installed. The distances from the wind pole to the nearby observatory buildings are 60, 25, and 65 m for SDZ, LAN, and LFS, respectively, to ensure that the air sample is minimally affected by human activities in the buildings. In 2010, new sampling towers of 50 and 80 m height were erected at LAN and LFS, respectively. In 2011, an 80 m sampling tower was built at SDZ. A second sampling inlet was installed at the top level of each tower, in addition to the previous 10 m high inlet. The air intake into each Picarro analyzer then switched between the 10 m and the top-level intake every 5 min at the three stations. Because of the short records available from the highest level at the three regional stations, we mainly discuss measurements from the 10 m intake. At WLG station, the air sample inlet is fixed at an 80 m height of an 89 m sampling tower located 15 m from the laboratory.

2.2 Measurement system

CRDS systems (G1301, Picarro Inc.) are used for continuous measurements of atmospheric CO_2 and CH_4. This type of instrument has been proven suitable for making precise measurement of CO_2 and CH_4 mole fraction since its response is both highly linear and very stable (Chen et al., 2010; Crosson, 2008). Air sample is delivered to the instrument by a vacuum pump (N022, KNF Neuberger, Freiburg-Munzingen, Germany) via a dedicated 10 mm o.d. sampling line (Synflex 1300 tubing, Eaton, OH, USA). Then the ambient air is filtered and pressurized at 1 atm. The ambient air is dried to a dew point of approximately $-60\,^{\circ}$C by passing it through a glass trap submerged in a $-70\,^{\circ}$C methanol bath (MC480D1, SP Industries, PA, USA). An automated sampling module equipped with a VICI 8 port multiposition valve is designed to sample from separate gas streams (standard gas cylinders and ambient air). The detailed schematic of the measurement setup is described in Fang et al. (2013). The residence time of air sample from the top of the inlets to inlet of Picarro is less than 30 s. The individual systems started service on 1 January 2009 at LAN, LFS, SDZ, and WLG and are still running. In this study, the analysis is restricted to the period of January 2009 to December 2011 period.

2.3 Calibration, quality control, and data processing

Carbon dioxide mole fractions are referenced to a working high standard (WH) and a working low standard (WL). Additionally, a calibrated cylinder filled with compressed ambient air is used as a target gas (T) to check the precision and stability of the system routinely. All standard gases are pressurized in 29.5 L treated aluminum alloy cylinders (Scott-Marrin Inc.) fitted with high-purity, two-stage gas regulators. The standard gases are calibrated with cylinders assigned by the WMO/GAW CO_2 Central Calibration Laboratory operated by NOAA/ESRL. All data are reported on the WMO X2007 scale (Zhao and Tans, 2006; Zhao et al., 1997). Calibration of the working standards and target gases is done at CMA's central laboratory in Beijing before and after use at the four stations. The two standards and target gas are analyzed by the system for 5 min every 12 h.

The discrete flask samples collected weekly at WLG have been measured by the Carbon Cycle Greenhouse Gases group (CCGG) of NOAA/ESRL in Boulder, CO, USA. Two flask samples were collected in series at 08:00 LT (local time) using glass flasks and a portable battery-powered sampling apparatus with a 5 m (a.g.l.) intake height (Dlugokencky et al., 1994). The samples were measured at NOAA using a non-dispersive infrared (NDIR) analyzer with a repeatability of approximately 0.1 ppm (Zhou et al., 2005). The average time between sampling and analysis is about 2 months. All CO_2 measurements are also tied to the WMO CO_2 scale X2007. The co-located NOAA flask program at WLG ensures that the long-term CMA in situ measurements can be routinely compared with an independent record.

Because of the dead volumes in the in situ sampling system, the response of the analyzer is usually not stable until

1 min after switching to a different gas source using the multiposition valve. Every gas cylinder (WH, WL, or T) was measured for 5 min and the data processing routine used the last 3 min of each 5 min segment to compute CO_2 mole fractions. The same is done for the ambient air data after switching in 5 min intervals from one sampling height to the other and after the reference gas measurements. The average of the last 3 min is used to represent the CO_2 concentration in current 5 min segment. The ambient measurements were calibrated using a linear two-point fit through the most recent standard gas measurements (WH and WL). Ambient CO_2 measurements were retained only during periods when the measurement of the most recent target gas (T) using this same calibration procedure was within ± 0.1 ppm of its assigned value. More than 97 % of the total 5 min average data points were retained for meeting this criterion at the four stations and treated as valid data.

After computing the CO_2 mole fractions, the valid data were manually inspected. Occasionally, analytical or sampling problems – including local influences such as nearby fires, vehicles, and cattle identified according to the station logbook entries made by the local operators – affected the observations. Those events were eliminated prior to the next processing steps. More than 97 % of valid 5 min data remained for each station after this filtering step. The 5 min data selected in that manner were then aggregated to hourly averages. To evaluate the seasonal cycle and peak-to-peak amplitude, we used the curve-fitting method described by Thoning et al. (1989). The data were first fitted to a function with three polynomial terms and four harmonic terms. Residuals from the function were then filtered (smoothed) in the time domain using two different low-pass filters (a Butterworth filter, which computes weighted averages over 1.07 years at full width at half maximum (FWHM) of the weighting function, and the second filter 1.5 months at FWHM). The smoothed residuals are then added to the function to obtain smoothed time series with the seasonal cycle removed (1.07 years FWHM) or representative of approximately monthly values for the second filter, as seen in Fig. 2. Except for special notes, the averaged values in this study are reported with 95 % confidence intervals (CI). The CO_2 mole fractions in this study are atmospheric CO_2 dry air mole fractions.

3 Results and discussions

3.1 Carbon dioxide data

Figure 2 shows the hourly averages of the processed ambient air CO_2 concentration at the four stations. The data gaps at WLG are due to a malfunction of the instrument. Valid flask sample pair measurements at WLG during the same period are also shown. To test the measurement quality of the Picarro system, differences between discrete flask measurements from NOAA ESRL and corresponding hourly CO_2 mole fractions from the Picarro instrument at WLG are studied. For the greater part of the time, differences between flasks and in situ systems vary by ± 1 ppm. The mean value of the difference (flask minus in situ) is 0.1 ± 0.1 ppm (95 % CI) for 168 sampling events (336 flasks). This result suggests that NOAA flask and CMA in situ measurements at WLG are in good agreement and the CMA calibration and quality control procedures are well implemented without generating systematic biases. The differences between the two data sets are likely due to the sampling height and method (Zhou et al., 2005). The discrete flask sampler collects air 5 m above the ground, while the in situ system is measuring air at 80 m. Due to unique topography at WLG station (located at the top of Mt. Waliguan in the Tibetan Plateau), the flask samples are collected at 08:00 LT (local time) before the updraft in the daytime may bring the local contaminations from the valley. The NOAA flask sampler collects air samples almost instantaneously (sampling period < 1 min), whereas the Picarro system generally has a continuous coverage during each hour. Thus, a part of the differences can be most likely explained by the atmospheric CO_2 fluctuations.

3.2 Mean diurnal cycles

The mean diurnal cycles of CO_2 variations in April, July, October, and January in all 3 years are used to represent the average variations in spring, summer, autumn, and winter, respectively. Only days containing 24-hourly averaged CO_2 mole fractions are used, because the day-to-day variations of CO_2 can be quite large. The mean diurnal variations are shown in Fig. 3. Generally, diurnal CO_2 variation is affected by two factors: local sources/sinks and short/medium-range transport (Artuso et al., 2009; Gerbig et al. 2006). In summer, the CO_2 diurnal variation has a similar phase between the sites, with peak values in the early morning and minima in afternoon. After sunrise, photosynthetic CO_2 uptake and mixing of near-surface air with lower concentrations aloft makes the CO_2 mole fractions decrease gradually and reach a stable minimum at about the period of 14:00 to 16:00 LT. In the late evening, when respiration dominates and the boundary layer becomes neutral or stable, CO_2 increases near the surface, and reaches a maximum at 06:00–07:00 LT in the morning, except at LFS, where the maximum concentration is observed at $\sim$ 05:00 LT. The earlier maximum at LFS is likely due to an earlier sunrise time.

The LAN station is located in the subtropics. Compared with the other three stations, variations of air temperature (yearly average: 14°) and solar radiation are relatively small during the year. As a result, photosynthetic/respiration fluxes are active (Kerang et al., 2004) in all seasons and diurnal CO_2 variations are thus significant throughout the year. The peak-to-peak mean diurnal amplitudes are 20.7 ± 5.0, 43.2 ± 6.4, 20.0 ± 4.0, and 8.3 ± 4.6 ppm for spring, summer, autumn, and winter, respectively. The larger amplitude in summer is

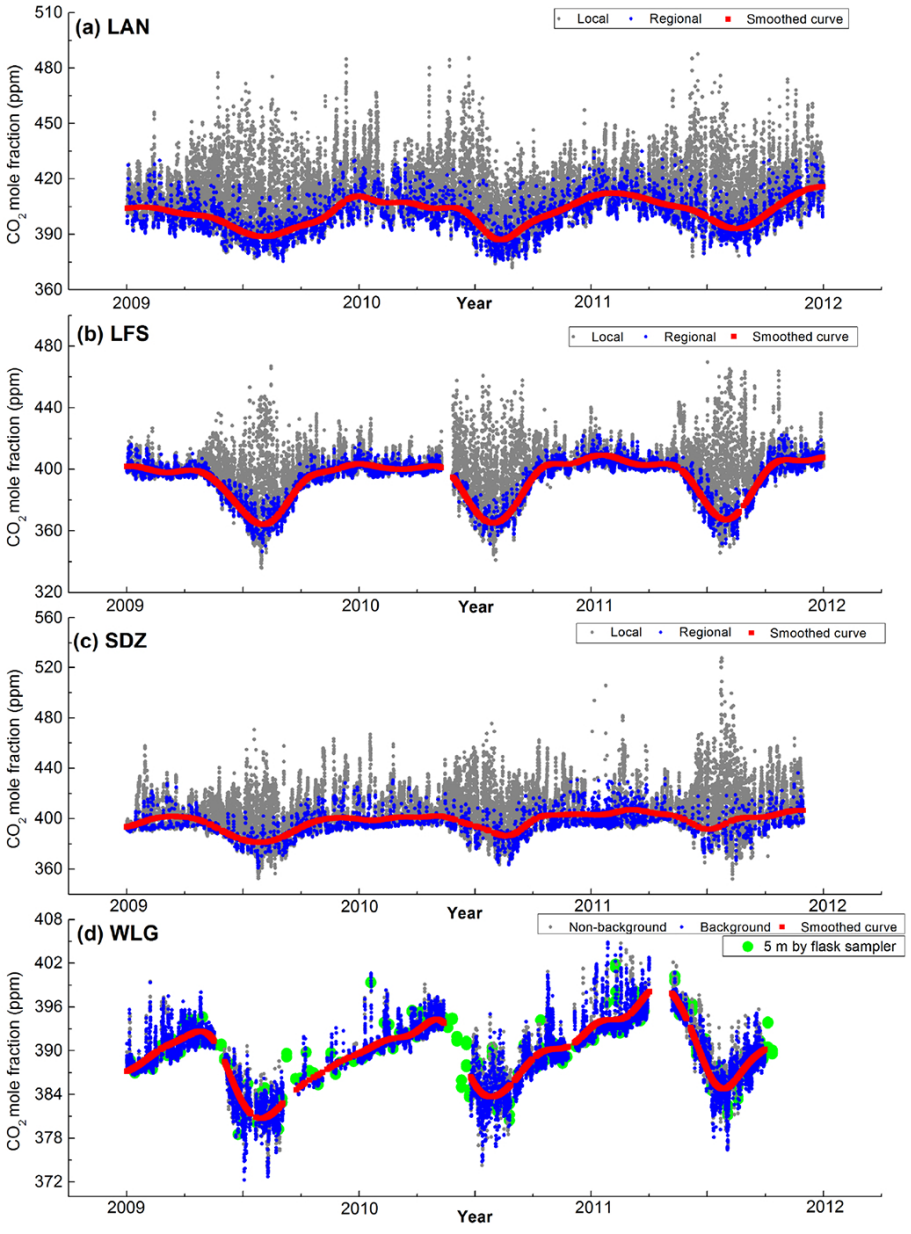

Fig. 2. Seasonal variations of hourly CO_2 mole fractions at **(a)** Lin'an (LAN), **(b)** Longfengshan (LFS), **(c)** Shangdianzi (SDZ), and **(d)** Mt. Waliguan (WLG). Grey dots are locally representative CO_2 mole fractions and the blue dots are regional or background records. See Sect. 3.5 for further details. The red dots are curve-fitted results to the regional records using the curve-fitting method by Thoning et al. (1989). The concentrations at LAN, LFS, and SDZ are from 10 m a.g.l. At WLG **(d)**, grey and blue dots are CO_2 concentration from 80 m a.g.l., and green dots denote discrete CO_2 flask pair measurement from the NOAA ESRL flask air-sampling program.

due to the higher temperature and solar radiation, which stimulate the assimilation in the daytime and respiration in the night.

Distinct CO_2 variations at LFS are also observed in summer. The diurnal amplitude is 50.6 ± 7.0 ppm, which is the largest among the four stations. This is probably due to the active CO_2 fluxes from nearby paddy rice fields and forests (Yue et al., 2005). The LFS station is located in the most important rice production area ($> 40\,000$ km^2) of China. In spring and autumn, the CO_2 diurnal variations are moderate, and display maxima in the morning and minima in the afternoon with a peak-to-peak amplitude of 4.5 ± 1.9 ppm in spring and 7.3 ± 4.8 ppm in autumn. There is no clear diurnal CO_2 variation in winter ($< 1.9 \pm 2.9$ ppm), which reflects weak local sources at LFS station.

The SDZ station exhibits complex CO_2 variations in the four seasons. In summer, the confidence intervals of the hourly averages (error bars in Fig. 3) are the highest among

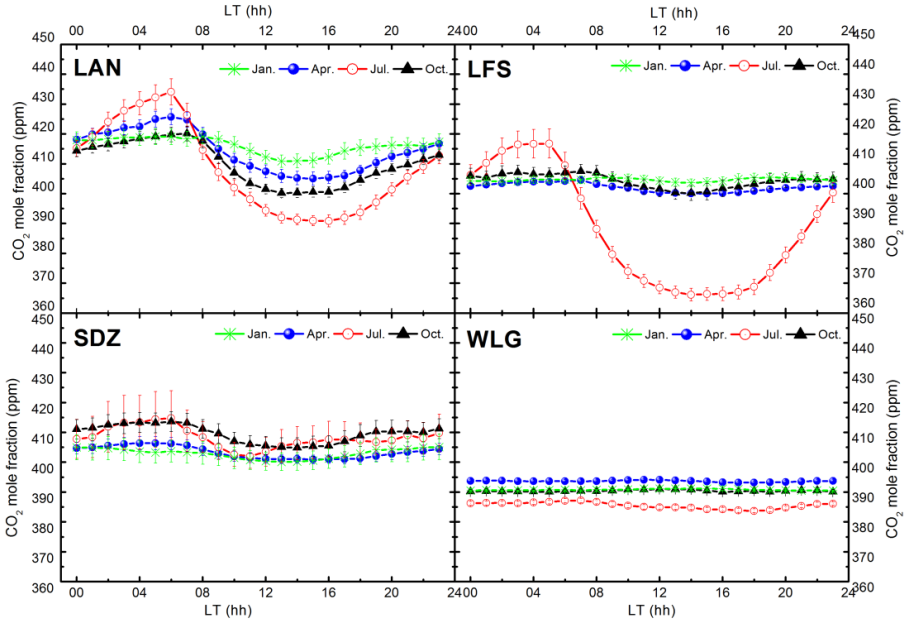

Fig. 3. Mean diurnal variations of CO_2 mole fractions in January, April, July, and October. Error bars indicate confidence intervals of 95 %. LAN, LFS, and SDZ data are sampled at 10 m a.g.l., while WLG data are sampled at 80 m a.g.l.

the four stations. The mean standard deviations for hourly CO_2 concentration are 9.5, 21.5, 15.9, and 12.7 ppm for spring, summer, autumn, and winter, respectively, which is much higher than for the other stations. These large values imply that the day-to-day variations of CO_2 are large compared to the periodic diurnal cycle. It can also be inferred that this site may be influenced by very nearby emissions. In spring and autumn, the diurnal variations have amplitudes of 5.5 ± 3.7 and 8.8 ± 6.7 ppm, respectively. The larger diurnal variation in autumn may be due to the straw burning in the northeastern China plain (Cao et al., 2008; Li et al., 2008). In summer and winter, the standard deviations of the hourly averages are so large that the uncertainty is larger than the discrepancy between peak and valley. As a result, the peak-to-peak daily amplitude cannot be calculated in these seasons.

The WLG high mountain station receives well-mixed air masses from the lower troposphere, with very small diurnal variability (see also Keeling et al., 1976). CO_2 are systematically lower than at the three regional near-surface stations. Diurnal cycles are small throughout the year with the largest intensity in summer, when a diurnal amplitude of 3.4 ± 1.4 ppm is recorded. Observed seasonal and diurnal variations are similar to those observed from 1994 to 2000 reported by Zhou et al. (2002).

3.3 Comparison of CO_2 mole fractions between different levels

Similar to the previous study (Fang et al., 2013), to understand the effect of local sources and sinks on observed CO_2 concentration, the diurnal variations of hourly discrepancy between 10 m and the top of the sampling tower (50 m for LAN and 80 m for LFS) during the two-level parallel observation period are shown in Fig. 4. The record for SDZ is too short (six months) and is not drawn. Generally, CO_2 mole fractions at 10 m are higher than the top levels. The CO_2 differences at LAN and LFS show distinct diurnal variations, with large positive values at night and smaller values in the daytime, partly driven by the coupling between respired CO_2 emitted at night that usually accumulates in a shallow stable nocturnal boundary layer and net CO_2 uptake and efficient vertical mixing during daytime. At night, the maximum differences are 4.8 ± 0.5 ppm for LAN and 7.6 ± 1.3 ppm for LFS. The larger difference at LFS reflects there are stronger sources near the LFS observatory. Nevertheless, the height of top level at LAN (50 m) may also contribute to the smaller difference. At midday, differences at the two regional stations are the smallest and relatively stable. The values are less than 0.2 ± 0.2 ppm from 10:00 to 16:00 LT at LAN and 0.3 ± 0.2 ppm from 09:00 to 16:00 LT at LFS. Given the CO_2 diurnal variations at the two regional stations, the observed CO_2 mole fractions during these periods should be the least influenced by local sources and sinks. These significant differences between 10 and 50/80 m due to the covariance of local vegetation fluxes with vertical mixing prevents inversion models to use nighttime data at 10 m for regional flux estimates. Data during daytime at 10 m could be used in inversions with a bias correction of 0.2 to 0.3 ppm relative to 50/80 m.

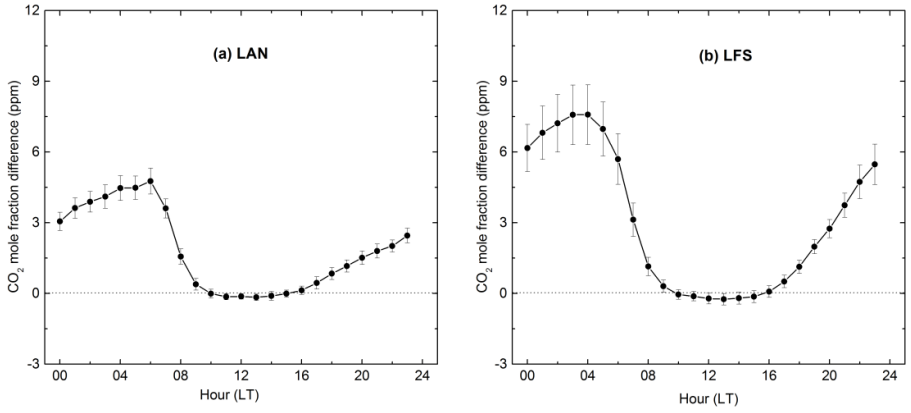

Fig. 4. Diurnal differences of hourly CO_2 mole fractions between 10 m and the top of each tower at the two regional stations. **(a)** LAN station, CO_2 concentration at 10 m minus 50 m. **(b)** LFS station, 10 m minus 80 m. Error bars indicate confidence intervals of 95 %.

3.4 Impact of local or regional sources on CO_2 concentration

In this study, we mainly focus on CO_2 concentration that is not obviously affected by very local sources and sinks ($\leq \sim 10$ km). As the three regional stations are located in an area of complex terrain, the observed CO_2 mole fractions are likely affected by very local sources for certain wind directions. At LAN, the town of Lin'an is located to the southwest (SW–SSW sector). As a result, observed CO_2 mole fractions are higher than the other directions in the four seasons (data not shown). Especially in autumn, the maximum enhancement relative to the seasonal average (407.5 ± 0.4 ppm) is 7.4 ± 1.6 ppm. Additionally, the charcoal factory located at 1.4 km north of the station may emit a large amount of CO_2 during manufacturing. At LFS, the small villages located to the north (~ 200 m) will affect the observed CO_2 mole fractions of the northern wind. This phenomenon is very obvious in winter, when local fossil fuel emission (coal for domestic heating) is stronger, with 3.6 ± 0.7 ppm above the average winter mean (404.6 ± 0.2 ppm). The SDZ station is located in an area with strong local sources in the vicinity of the site. Besides the small village located at about 0.8 km to the south, the railway used by diesel-driven trains runs from southwest to northwest, ~ 0.6 km away from the station, may contribute to the CO_2 mole fractions during the whole year.

Similar to the previous study by Zhou et al. (2004), the surface wind is used to identify the possible local and regional sources at WLG. From the wind-rose distribution patterns of CO_2 mole fractions on 16 directions (Fig. 5), it can be seen that surface winds originating from the NE–ENE sector are associated with CO_2 enhancements, with a maximum value of 3.6 ± 1.0 ppm above the seasonal average (391.4 ± 0.1 ppm) in winter. This likely reflects air masses exposed to regions with higher population density. Furthermore, Tang et al. (1999) studied the relationship of black carbon (BC) with surface winds and long-range transport and also found that the highest BC concentrations occur with air masses originating from the NE–NNE sector. They attributed these elevated BC concentrations to remote emissions from the Yellow River canyon industrial area (including cities of Xining, Lanzhou, etc.), 500 km to the northeast of WLG. This phenomenon is more obvious in winter, when the uptake by vegetation on the transporting path is very weak. In winter, in addition to NE–ENE sector, CO_2 concentration on E–ESE–SE sectors is also obviously higher. This is probably due to the emissions from coal burning for heating in Guide County, which is 5 km away to east of the station.

In order to further identify the effect of local sources and sinks, hourly CO_2 mole fractions during the 3 years were calculated for different wind speeds (Beaufort scale): scale 0: $< 0.3\,m\,s^{-1}$; scale 1: 0.3 to $1.5\,m\,s^{-1}$; scale 2: 1.6 to $3.3\,m\,s^{-1}$; scale 3: 3.4 to $5.4\,m\,s^{-1}$; scale 4: 5.5 to $7.9\,m\,s^{-1}$; scale 5: 8.0 to $10.7\,m\,s^{-1}$; scale 6: 10.8 to $13.8\,m\,s^{-1}$, $\geq$; and scale 7: $\geq 13.9\,m\,s^{-1}$. Results show that the observed CO_2 concentration is strongly dependent on the wind speed at the four stations. At LAN, LFS, and SDZ, lower CO_2 mole fractions are always accompanied with higher wind speed in the four seasons, even in summer when the local photosynthesis is very active. These results prove that higher wind speed (and longer range transport) may dilute the very local emissions. From the yearly average, the average CO_2 mole fractions are 416.2 ± 1.0, 402.7 ± 3.9, and 411.0 ± 1.3 ppm, respectively, in calm conditions (scale 0). When the wind speed is Beaufort scale 5, the average CO_2 concentrations are 397.1 ± 3.5, 397.2 ± 1.3, and 398.9 ± 1.4 ppm for LAN, LFS, and SDZ, respectively. For WLG, in winter and spring, decreasing CO_2 concentration is also observed with increasing wind speed. However, during summer and autumn, an opposite behavior is observed. CO_2 increases with increasing wind speed, which may reflect that the local photosynthesis dilutes the anthropogenic signals. For example, in summer, the average CO_2 mole fraction is 384.5 ± 1.5 ppm for calm conditions (scale 0) and 388.2 ± 0.9 ppm at wind scale 7.

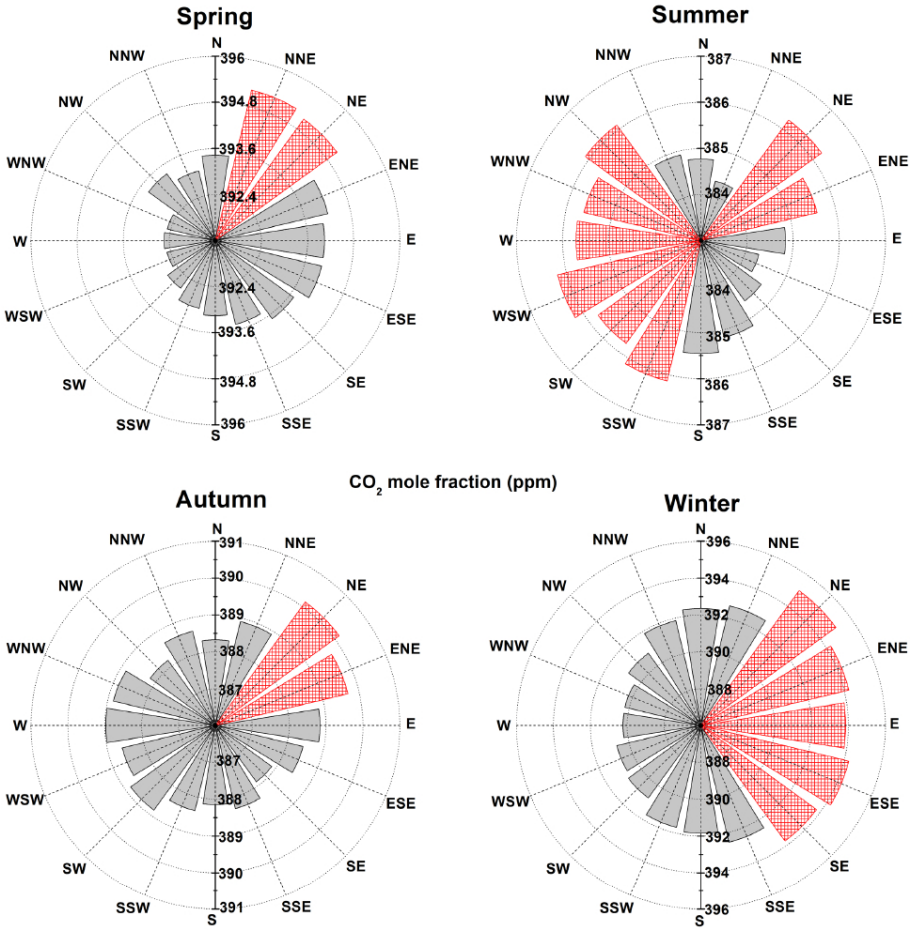

Fig. 5. Seasonal hourly CO_2 mole fractions on 16 horizontal wind directions at WLG. The light-grey bars denote CO_2 mole fractions from wind sectors considered to be background representative, while the red hatched bars denote CO_2 mole fractions that are likely to be influenced by local/regional sources.

The higher wind speed may bring emissions from a larger regional area (such as emissions from the northwest of China, e.g., Xining city of Qinghai province) and contribute to the higher CO_2 mole fractions.

3.5 Evaluation of "regional" or "background" mole fractions

A data-filtering approach was applied to the CO_2 concentration at the three regional stations (SDZ, LFS and LAN) in order to divide the time series into periods under predominantly "local" and "regional" influence. Regional episodes rather represent CO_2 mole fractions driven primarily by distant sources and sinks ($> \sim 10$ km), while the CO_2 mole fractions during local episodes are more strongly influenced by local sources and sinks ($\leq \sim 10$ km). Based on the analysis of the observed diurnal cycles and the comparison of the CO_2 mole fractions at the different inlet heights (Sects. 3.2 and 3.3), hourly CO_2 concentration was considered to be regionally representative during daytime hours, i.e., from 10:00 to 16:00 LT at LAN and during 09:00 and 16:00 LT at LFS and SDZ.

However, even during midday there was still a mixture of regional and local evens because the local sources and sinks are strong at the regional stations. To get "the least influenced" CO_2 concentration, the CO_2 mole fractions were further flagged when surface winds from the sectors with local sources were located (see discussion in Sect. 3.4). They were SSW–SW and N sector for LAN, N for LFS, and S–SSW–…–NNW for SDZ. In addition, at low wind speeds, local emissions and sinks typically play a larger role on observed CO_2 mole fractions than high wind speed. Thus for LAN, LFS, and SDZ, CO_2 mole fractions were rejected when surface winds speeds were below 1.5 m s^{-1} (scale 0 and 1).

At WLG, CO_2 record was split into "background" and "regional/local" events according to the previous regime used by Zhou et al. (2004). Firstly, data from 06:00 to 07:00 LT in summer were considered to be under local influence when the observed CO_2 mole fractions were about 1.9 ± 0.8 ppm higher than the seasonal average

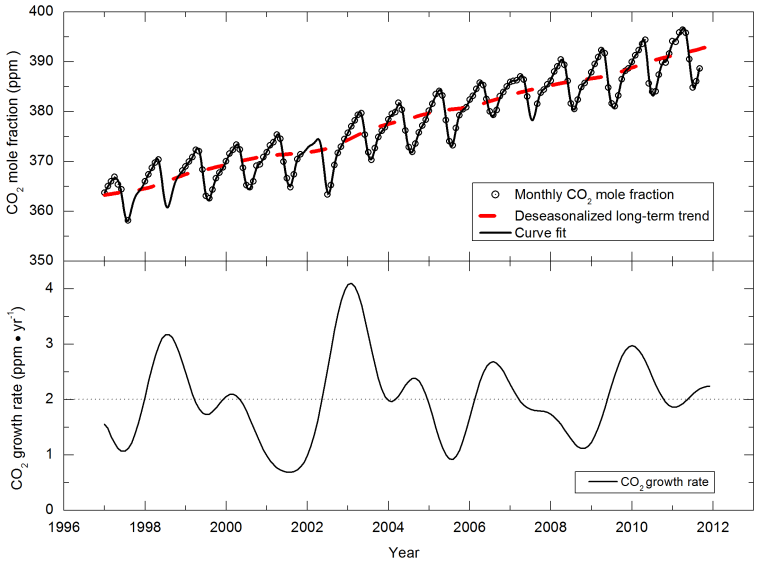

Fig. 6. Top panel: monthly CO_2 mole fractions (open circles) at WLG from 1997 to 2011, as well as the curve fit (black curve) and deseasonalized long-term trend (red dash line). Bottom panel: the annual growth rate of CO_2. The trend, curve fit, and annual growth rate are calculated by the curve-fitting method of Thoning et al. (1989).

(385.2 ± 0.1 ppm). Secondly, the "regionally or local" influenced sectors there were the NNE to NE sector for spring, the NE to ENE and SSW to NW sector for summer, the NE to ENE sector for autumn, and the NE to SE sector for winter (Fig. 5). The corresponding CO_2 mole fractions were flagged when surface winds were from these directions. Finally, as discussed above, the higher wind speeds might also transport emissions from the broader region and induce higher CO_2 mole fractions. Thus the CO_2 mole fractions were excluded to be background when surface wind speeds were below scale 1 or above scale 6.

After the three steps filter, one subset for each station is considered to be minimally influenced by local sources, measured during so-called "regional" events (for WLG, they are "background" events). For the three regional stations, about 16.6, 23.9, and 14.4 % of hourly CO_2 mole fractions are selected as regionally for LAN, LFS, and SDZ, respectively. On the other hand, the large ratios of local events (possibly affected by local sources and sinks) prove that local sources and sinks strongly affect the observed CO_2 concentration at 10 m intakes. The background events at WLG account for about 62.6 % of the total hourly mole fractions, which reflects that the observations at WLG (at 80 m intake height) represent well-mixed air masses from the lower troposphere.

3.6 Yearly growth rates

We used the curve-fitting method described by Thoning et al. (1989) to extract the trends at the four stations. The filtered CO_2 mole fractions at the four stations all show positive trends in the last 3 years. The growth rates of regionally representative CO_2 at the three regional stations are 3.7 ± 1.2, 2.7 ± 0.8, and 3.5 ± 1.6 ppm yr^{-1} (1σ) for LAN, LFS, and SDZ respectively, which are all higher than the global values (2.3 ppm from 2009 to 2010, and 2.0 ppm from 2010 to 2011) (WMO Greenhouse Gas Bulletin, 2011, 2012) and also higher than the average of the past decade (~ 2.0 ppm yr^{-1}) (WMO, 2012). Especially at LAN and SDZ station, the values almost double the global average, which implies that the emissions at the Yangtze Delta area and the North China Plain are growing rapidly in recent years. Using a similar method, the growth rates of the locally representative CO_2 mole fractions are calculated to be 3.2 ± 3.0, 3.4 ± 1.0, and 4.2 ± 1.9 ppm yr^{-1} (1σ) for LAN, LFS, and SDZ, respectively, which are also obviously higher than the global average.

At WLG, the average growth rate of CO_2 in the last 3 years is 2.2 ± 0.8 ppm yr^{-1} (1σ). Figure 6 illustrates the monthly CO_2 mole fractions in the last 15 years (from 1997 to 2011) and the deseasonalized long-term trend at this station. The variation shows that CO_2 concentration reached a new high of 389.5 ± 1.9 ppm in 2010, which is about 0.5 ppm higher than the global average in 2010 and 25.6 ppm higher than the value at WLG in 1997. The long-term trend displayed a positive growth in the last 15 years with a value of ~ 2.0 ppm yr^{-1}. As a WMO/GAW global station, the growth rate variation at WLG is similar to the global average with four distinct peaks (Fig. 6) in the periods 1998, 2003/2004, 2006, and 2010/2011 (WMO, 2012). The former two peaks are very likely linked to the El Niño–Southern Oscillation

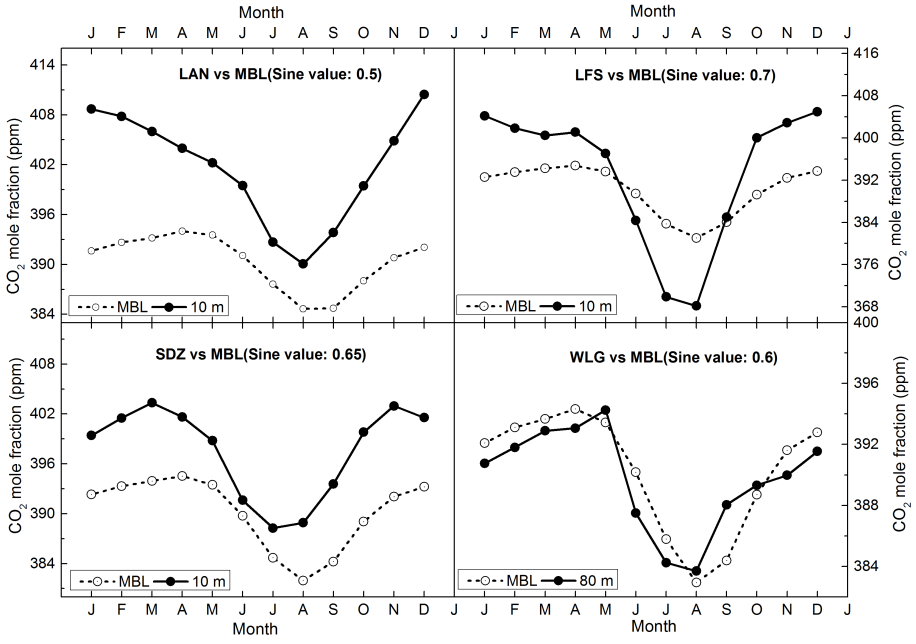

Fig. 7. Variations of monthly CO_2 mole fractions at LAN, LFS, SDZ, and WLG during the period 2009 to 2011. Also compare to the surface values at similar latitudes from the MBL reference (Conway et al., 2012b). LAN compares to those of sine of latitude value 0.5, WLG with 0.6, SDZ with 0.65, and LFS with 0.7. The closed circles and solid line denote the monthly averaged CO_2 concentration at the four stations. The open circles and dashed lines denote the monthly average CO_2 values from the MBL reference. The data in this figure are smoothed from the filtered CO_2 mole fractions (regionally representative for LFS, SDZ, LAN, and background for WLG) by the curve-fitting method of Thoning et al. (1989).

(ENSO), which are very commonly seen at other stations (Artuso et al., 2009).

3.7 Seasonal variations of regional CO_2 mole fractions

We also used the curve-fitting method described by Thoning et al. (1989) to get the seasonal variations (Figs. 2 and 7) of the filtered CO_2 mole fractions (regionally representative for LFS, SDZ, LAN, and background for WLG) at the four stations. For comparison, simulated surface CO_2 concentration at similar latitude to the four stations from the marine boundary layer (MBL) reference computed by NOAA/GMD (LAN; sine of latitude value: 0.5; WLG, 0.6; SDZ, 0.65; and LFS, 0.7) (Conway et al., 2012b) are also overlaid. Seasonal cycle of CO_2 in the Northern Hemisphere is mainly dominated by exchange with the land biosphere and thus characterized by rapid decreases from June to August and large returns from September to December (Nevison et al., 2008; WMO, 2012). At the four stations, minimum CO_2 concentration all occur in August, which are similar to the Northern Hemisphere (MBL), and the time of occurrence at WLG is consistent with the previous study by Zhou et al. (2005). However, the seasonal CO_2 maximum occurrence times vary substantially, ranging from December for LFS and LAN, to March for SDZ, and to May for WLG. This difference is thought to be caused not only by regionally different terrestrial ecosystems and human activities but also by local meteorological conditions (Zhang et al., 2008). The high CO_2 mole fractions observed at LFS in winter is likely due to regional coal burning (heating) and biomass burning (agricultural fires), which begins in October in the northeastern China plain. LAN is located in the Yangtze Delta area, which is the economically most developed region in China. In winter, in addition to the lower boundary layer, the increase of fossil fuel consumption may also partly contribute to the higher CO_2 mole fractions. The maximum CO_2 mole fraction occurrence time at WLG, a global WMO background site, agrees with the MBL and those observed at sites of similar latitudes (Nakazawa et al., 1993; Riley et al., 2005; Thoning et al., 1989).

At LAN, the monthly CO_2 mole fractions are obviously higher than the similar MBL references during the whole year, with an average monthly difference of 11.3 ± 4.3 (1σ) ppm, which means that the LAN area (Yangtze Delta area) is a very strong source of regional atmospheric CO_2. Similarly, the CO_2 mole fractions at SDZ are also generally higher than the concentration at similar latitude (sine of latitude value: 0.65) with a mean of 7.4 ± 2.7 ppm (1σ). Both stations display a larger difference to the MBL in the autumn and winter period and smaller values in summer. The CO_2 mole fractions at LFS are strongly affected by regional vegetation canopy in summer. As a result, CO_2 mole fractions are apparently lower than the MBL reference during the same

Table 2. Seasonal average CO_2 concentration and amplitude from the regional or background data sets.

Season	LAN (ppm)	LFS (ppm)	SDZ (ppm)	WLG (ppm)
Spring (Mar–May)	403.6 ± 0.5	399.6 ± 0.2	399.9 ± 0.5	393.1 ± 0.1
Summer (Jun–Aug)	392.7 ± 0.5	375.2 ± 0.7	385.9 ± 0.9	384.5 ± 0.2
Autumn (Sep–Nov)	398.0 ± 0.6	395.3 ± 0.5	396.6 ± 0.6	388.5 ± 0.1
Winter (Dec–Feb)	407.9 ± 0.6	403.0 ± 0.3	399.2 ± 0.5	390.9 ± 0.1
Peak-to-peak amplitude	19.1 ± 1.8	35.5 ± 1.1	15.3 ± 2.6	10.4 ± 0.4

Table 3. Comparison of yearly CO_2 mole fractions with other WMO/GAW stations.

Station*	Year	LAN	LFS	SDZ	WLG	RYO	MLO	JFJ
Latitude		30.18° N	44.73° N	40.65° N	36.3° N	39.03° N	19.54° N	46.55° N
Longitude		119.44° E	127.6° E	117.12° E	100.9° E	141.82° E	155.58° E	7.99° E
Altitude (m a.s.l.)		139	331	293	3816	260	3397	3580
Annual mean (ppm)	2009	397.4 ± 3.4	389.9 ± 7.1	392.4 ± 4.1	387.2 ± 2.1	389.8 ± 2.9	387.4 ± 1.1	388.2 ± 2.1
Annual mean (ppm)	2010	400.7 ± 4.4	393.2 ± 7.3	395.9 ± 3.7	389.5 ± 1.9	393.5 ± 2.1	389.8 ± 1.2	390.7 ± 2.1
Annual mean (ppm)	2011	404.2 ± 3.9	395.5 ± 7.7	397.8 ± 3.5	–**	394.3 ± 2.8	391.6 ± 1.0	392.2 ± 2.0

* See text (and http://gaw.empa.ch/gawsis/default.asp) for station name acronyms and other information. ** The years containing less than 12 months of data are not calculated.

period, with the maximum difference of -15.1 ± 5.8 ppm (1σ), which indicates that the LFS area may act as a sink of regional CO_2 in the summer. In the other seasons, similar to LAN and SDZ, CO_2 concentration is also obviously higher than the MBL references. Because WLG is located at a high altitude and in a remote area, the observed CO_2 concentration is close to the MBL references.

Because of the strong uptake by the rice plants and forest during growing season in the northeastern China plain, CO_2 mole fractions at LFS are extremely low in the summer and the peak-to-peak amplitude reaches to 35.5 ± 1.1 ppm (Table 2), which is the highest among the four stations. The amplitude at LFS in this study is also much higher than that (19.3 ± 4.1 ppm) by Zhang et al. (2008) during the period of 2003 to 2006. However, they used discrete flask sampling method, which might underestimate the value. CO_2 concentration at WLG is generally lower than those observed at the three regional stations and the seasonal peak-to-peak amplitude is 10.4 ± 0.4 ppm, which is close to similar MBL value (~ 11.4 ppm; sine of latitude value: 0.6) and the previous study (10.5 ppm) by Zhou et al. (2005).

Table 3 illustrates the annual CO_2 concentration at the four stations. For comparison, we also present the CO_2 mole fractions from Mauna Loa in the United States (MLO) (Conway et al., 2012a), Jungfraujoch in Switzerland (JFJ), and Ryori in Japan (RYO) during the same period. MLO and JFJ are WMO/GAW global measurement stations. RYO is GAW regional measurement station. The average regional CO_2 mole fractions at LAN, LFS, and SDZ are obviously higher than the global mean (~ 389 ppm in 2010 and 390.9 ± 0.1 ppm in 2011) (WMO Greenhouse Gas Bulletin, 2011, 2012) and other WMO/GAW global stations such as MLO and JFJ. Compared with the CO_2 concentration observed at other regional stations (such as RYO) close to China, CO_2 mole fractions at the three regional stations are also higher, proving that the stations in China are influenced by (domestic) CO_2 emissions. The highest annual mean CO_2 concentration is observed at LAN of 404.2 ± 3.9 ppm in 2011. This is due to the megacities (Shanghai and Hangzhou) in this region as well as the many industrial sources such as coal-fired power plants (Wang et al., 2006; Zeng et al., 2008). The strong uptake by local vegetation in summer obviously decreases the atmospheric CO_2 mole fractions at LFS. As a result, the annual mole fractions at this station are relatively lower than those at LAN and SDZ.

4 Conclusions

Atmospheric CO_2 measurements made at four WMO/GAW stations in China have been reported. The diurnal patterns, atmospheric trends, and seasonal variations at each site were discussed. The results indicate that CO_2 mole fractions from 10 m a.g.l. at the three regional stations (LAN, LFS, and SDZ) are affected by local sources. Measurements from WLG are representative of the Tibetan Plateau.

The CO_2 mole fractions at the three regional stations are generally higher than the values at respective similar latitudes from MBL references. CO_2 concentration at LAN is representative of the Yangtze Delta area, China, and is the highest among the four stations. Atmospheric CO_2 at LFS are strongly affected by local vegetation (paddy rice and forest) in summer. As a result, it has the lowest CO_2 concentration in summer and the highest seasonal amplitude among the four stations. The SDZ station is located in an area with complex topography. The day-to-day variation of atmospheric CO_2 is quite large. The seasonal CO_2 variations at WLG are small and similar to other GAW global stations (such as MLO in the USA, and JFJ in Switzerland) with peak concentration observed in spring.

In this study, we present continuous atmospheric CO_2 measurements from 2009 to 2011. The relatively short 3-year record may introduce bias in our analysis of the seasonal variations and estimates of trends. However, the present analysis gives a first very valuable insight into the evolution and distribution of CO_2 mole fractions across China. To better understand atmospheric CO_2 in China, a more extensive CO_2 observing network and longer period of in situ measurements is required.

Acknowledgements. We express our great thanks to the staff at Lin'an, Longfengshan, Shangdianzi, and Waliguan station who have contributed to the system installation and maintenance at the stations. This work is supported by the National Natural Science Foundation of China (program no. 41175116), the National Key Basic Research Program (no. 2010CB950601), the International S & T Cooperation Program of the MOST (no. 2011DFA21090), and the CMA operational fund (2012Y003). The data used in this study will be available to the public within the China Meteorological Administration (CMA) policy.

Martin Steinbacher acknowledges funding through the GAW Quality Assurance/Science Actitity Centre (QA/SAC) Switzerland, supported by MeteoSwiss.

We thank NOAA ESRL, the Japan Meteorological Agency (JMA), and the University of Bern for providing monthly CO_2 data from Mauna Loa (Hawaii) in the US, Ryori in Japan, and Jungfraujoch in Switzerland from 2009 to 2011. The monthly data are downloaded from World Data Centre for Greenhouse Gases (WDCGG).

Finally, we also greatly appreciate NOAA ESRL for long-term cooperation on the WLG flask air sampling program and NDIR in situ measurement program and Ken Massarie for helping us with the data comparison.

Edited by: C. Gerbig

References

Artuso, F., Chamard, P., Piacentino, S., Sferlazzo, D. M., Silvestri, L. D., Sarra, A. D., Meloni, D., and Monteleone, F.: Influence of transport and trends in amtospheric CO_2 at Lampedusa, Atmos. Environ., 43, 3044–3051, 2009.

Ballantyne, A. P., Alden, C. B., Miller, J. B., Tans, P. P., and White, J. W. C.: Increase in observed net carbon dioxide uptake by land and oceans during the past 50 years, Nature, 488, 70–73, 2012.

Broquet, G., Chevallier, F., Bréon, F.-M., Kadygrov, N., Alemanno, M., Apadula, F., Hammer, S., Haszpra, L., Meinhardt, F., Morguí, J. A., Necki, J., Piacentino, S., Ramonet, M., Schmidt, M., Thompson, R. L., Vermeulen, A. T., Yver, C., and Ciais, P.: Regional inversion of CO_2 ecosystem fluxes from atmospheric measurements: reliability of the uncertainty estimates, Atmos. Chem. Phys., 13, 9039–9056, doi:10.5194/acp-13-9039-2013, 2013.

Cao, G., Zhang, X., Wang, Y., and Zheng, F.: Estimation of emissions from field burning of crop straw in China, Chinese Sci. Bull., 53, 784–790, 2008.

Chen, H., Winderlich, J., Gerbig, C., Hoefer, A., Rella, C. W., Crosson, E. R., Van Pelt, A. D., Steinbach, J., Kolle, O., Beck, V., Daube, B. C., Gottlieb, E. W., Chow, V. Y., Santoni, G. W., and Wofsy, S. C.: High-accuracy continuous airborne measurements of greenhouse gases (CO_2 and CH_4) using the cavity ring-down spectroscopy (CRDS) technique, Atmos. Meas. Tech., 3, 375–386, doi:10.5194/amt-3-375-2010, 2010.

Chevallier, F., Deutscher, N. M., Conway, T. J., Ciais, P., Ciattaglia, L., Dohe, S., Fröhlich, M., Gomez-Pelaez, A. J., Griffith, D., Hase, F., Haszpra, L., Krummel, P., Kyrö, E., Labuschagne, C., Langenfelds, R., Machida, T., Maignan, F., Matsueda, H., Morino, I., Notholt, J., Ramonet, M., Sawa, Y., Schmidt, M., Sherlock, V., Steele, P., Strong, K., Sussmann, R., Wennberg, P., Wofsy, S., Worthy, D., Wunch, D., and Zimnoch, M.: Global CO_2 fluxes inferred from surface air-sample measurements and from TCCON retrievals of the CO_2 total column, Geophys. Res. Lett., 38, L24810, doi:10.1029/2011GL049899, 2011.

Conway, T. J., Lang, P. M., and Masarie, K. A.: Atmospheric Carbon Dioxide Dry Air Mole Fractions from the NOAA ESRL Carbon Cycle Cooperative Global Air Sampling Network, 1968–2011, Version: 2012-08-15, ftp://ftp.cmdl.noaa.gov/ccg/co2/flask/event/ (last access: 13 May 2013), 2012a.

Conway, T. J., Masarie, K. A., Lang, P. M., and Tans, P. P.: NOAA greenhouse gas reference from atmospheric carbon dioxide dry air mole fractions from the NOAA ESRL Carbon Cycle Cooperative Global Air Sampling Network, Path: ftp://ftp.cmdl.noaa.gov/ccg/co2/flask/ (last access: 13 May 2013), 2012b.

Crosson, E. R.: A cavity ring-down analyzer for measuring atmospheric levels of methane, carbon dioxide, and water vapor, Appl. Phys. B, 92, 403–408, 2008.

Dlugokencky, E. J., Steele, L. P., Lang, P. M., and Masarie, K. A.: The growth rate and distribution of atmospheric methane, J. Geophys. Res., 99, 17021–17043, 1994.

Dlugokencky, E. J., Steele, L. P., Lang, P. M., and Masarie, K. A.: Atmospheric CH_4 at Mauna Loa and Barrow Observatories: presentation and analysis of in in situ measurements, J. Geophys. Res., 100, 23103–23113, 1995.

Fang, S. X., Zhou, L. X., Masarie, K. A., Xu, L., and Rella, C. W.: Study of atmospheric CH_4 mole fractions at three WMO/GAW stations in China, J. Geophys. Res., 118, 4874–4886, 2013.

Fu, Y., Zheng, Z., Yu, G., Hu, Z., Sun, X., Shi, P., Wang, Y., and Zhao, X.: Environmental influences on carbon dioxide fluxes over three grassland ecosystems in China, Biogeosciences, 6, 2879-2893, 2009, http://www.biogeosciences.net/6/2879/2009/.

Gerbig, C., Lin, J. C., Munger, J. W., and Wofsy, S. C.: What can tracer observations in the continental boundary layer tell us about surface-atmosphere fluxes?, Atmos. Chem. Phys., 6, 539–554, doi:10.5194/acp-6-539-2006, 2006.

GLOBALVIEW-CO_2: Cooperative Atmospheric Data Integration Project – Carbon Dioxide, NOAA ESRL, Boulder, Colorado, available at: http://www.esrl.noaa.gov/gmd/ccgg/globalview/ (last access: 3 January 2013), 2012.

Gourdji, S. M., Mueller, K. L., Yadav, V., Huntzinger, D. N., Andrews, A. E., Trudeau, M., Petron, G., Nehrkorn, T., Eluszkiewicz, J., Henderson, J., Wen, D., Lin, J., Fischer, M., Sweeney, C., and Michalak, A. M.: North American CO_2 exchange: inter-comparison of modeled estimates with results from a fine-scale atmospheric inversion, Biogeosciences, 9, 457–475, doi:10.5194/bg-9-457-2012, 2012.

Guan, D., Liu, Z., Geng, Y., Lindner, S., and Hubacek, K.: The gigatonne gap in China's carbon dioxide inventories, Nat. Clim. Change, 2, 672–675, doi:10.1038/nclimate1560, 2012.

Houghton, R. A.: Revised estimates of the annual net flux of carbon to the atmosphere from changes in land use and land management 1850–2000, Tellus B, 55, 378–390, 2003.

IPCC – Intergovernmental Panel on Climate Change: Climate Change 2007: The Physical Science Basis, Contribution of Working Group I to the Fourth Assessment, Report of the Intergovernmental Panel on Climate Change, edited by: Solomon, S., Qin, D., Manning, M., Chen, Z., Marquis, M., Averyt, K. B., Tignor, M., and Miller, H. L., Cambridge Univ. Press, New York, 2007.

Keeling, C. D.: Global observations of atmospheric CO_2, in: The Global Carbon Cycle, NATO ASI Series, vol. 15, edited by: Heimann, M., Springer-Verlag, New York, 1–30, 1993.

Keeling, C. D., Bacastow, R. B., Bainbridge, A., Ekdahl Jr., C. A., Guenther, P. R., Waterman, L. S., and Chin, J. F.: Atmospheric carbon dioxide variations at Mauna Loa Observatory, Hawaii, Tellus, 28, 538–551, 1976.

Keeling, R. F.: Recording earth's vital signs, Science, 319, 1771–1772, 2008.

Kerang, L., Wang, S., and Cao, M.: Vegetation and soil carbon storage in China, Sci. China Ser. D, 47, 49–57, 2004.

Lei, H. M. and Yang, D. W.: Seasonal and interannual variations in carbon dioxide exchange over a cropland in the North China Plain, Global Change Biol., 16, 2944–2957, 2010.

Le Quéré, C., Andres, R. J., Boden, T., Conway, T., Houghton, R. A., House, J. I., Marland, G., Peters, G. P., van der Werf, G. R., Ahlström, A., Andrew, R. M., Bopp, L., Canadell, J. G., Ciais, P., Doney, S. C., Enright, C., Friedlingstein, P., Huntingford, C., Jain, A. K., Jourdain, C., Kato, E., Keeling, R. F., Klein Goldewijk, K., Levis, S., Levy, P., Lomas, M., Poulter, B., Raupach, M. R., Schwinger, J., Sitch, S., Stocker, B. D., Viovy, N., Zaehle, S., and Zeng, N.: The global carbon budget 1959–2011, Earth Syst. Sci. Data, 5, 165–185, doi:10.5194/essd-5-165-2013, 2013.

Li, L., Wang, Y., Zhang, Q., Li, J., Yang, X., and Jin, J.: Wheat straw burning and its associated impacts on Beijing air quality, Sci. China Ser. D, 51, 403–414, 2008.

Liu, L., Zhou, L., Zhang, X., Wen, M., Zhang, F., Yao, B., and Fang, S.: The characteristics of atmospheric CO_2 concentration variation of the four national background stations in China, Sci. China, Ser. D, 52, 1857–1863, 2009.

Marland, G.: Emissions accounting: China's uncertain CO_2 emissions, Nat. Clim. Change, 2, 645–646, 2012.

Nakazawa, T., Morimoto, S., Aoki, S., and Tanaka, M.: Time and space variations of the carbon isotopic ratio of tropospheric carbon dioxide over Japan, Tellus B, 45, 258–274, 1993.

Necki, J., Schmidt, M., Rozanski, K., Zimnoch, M., Korus, A., Lasa, J., Graul, R., and Levin, I.: Six-year record of atmospheric carbon dioxide and methane at a high-altitude mountain site in Poland, Tellus B, 55, 94–104, 2003.

Nevison, C. D., Mahowald, N. M., Doney, S. C., Lima, I. D., van der Werf, G. R., Randerson, J. T., Baker, D. F., Kasibhatla, P., and McKinley, G. A.: Contribution of ocean, fossil fuel, land biosphere, and biomass burning carbon fluxes to seasonal and interannual variability in atmospheric CO_2, J. Geophys. Res., 113, G01010, doi:10.1029/2007JG000408, 2008.

Peters, G. P., Minx, J. C., Weber, C. L., and Edenhofer, O.: Growth in emission transfers via international trade from 1990 to 2008, P. Natl. Acad. Sci. USA, 108, 8903–8908, 2011.

Peters, G. P., Marland, G., Le Quéré, C., Boden, T., Canadell, J. G., and Raupach, M. R.: Rapid growth in CO_2 emissions after the 2008–2009 global financial crisis, Nat. Clim. Change, 2, 2–4, 2012.

Peters, W., Jacobson, A. R., Sweeney, C., Andrews, A. E., Conway, T. J., Masarie, K., Miller, J. B., Bruhwiler, L. M. P., Pétron, G., Hirsch, A. I., Worthy, D. E. J., van der Werf, G. R., Randerson, J. T., Wennberg, P. O., Krol, M. C., and Tans, P. P.: An atmospheric perspective on North American carbon dioxide exchange: CarbonTracker, P. Natl. Acad. Sci. US , 104, 18925–18930, doi:10.1073/pnas.0708986104, 2007.

Peylin, P., Law, R. M., Gurney, K. R., Chevallier, F., Jacobson, A. R., Maki, T., Niwa, Y., Patra, P. K., Peters, W., Rayner, P. J., Rödenbeck, C., van der Laan-Luijkx, I. T., and Zhang, X.: Global atmospheric carbon budget: results from an ensemble of atmospheric CO_2 inversions, Biogeosciences, 10, 6699–6720, doi:10.5194/bg-10-6699-2013, 2013.

Riley, W. J., Randerson, J. T., Foster, P. N., and Lueker, T. J.: Influence of terrestrial ecosystems and topography on coastal CO_2 measurements: A case study at Trinidad Head, California, J. Geophys. Res., 110, G01005, doi:10.1029/2004JG000007, 2005.

Sirignano, C., Neubert, R. E. M., Rödenbeck, C., and Meijer, H. A. J.: Atmospheric oxygen and carbon dioxide observations from two European coastal stations 2000–2005: continental influence, trend changes and APO climatology, Atmos. Chem. Phys., 10, 1599–1615, doi:10.5194/acp-10-1599-2010, 2010.

Tang, J., Wen, Y. P., and Zhou, L. X.: Observational study of black carbon aerosol in western China, J. Appl. Meteorol. Sci., 10, 160–170, 1999.

Tang, X., Liu, S., Zhou, G., Zhang, D., and Zhou, C.: Soil-atmospheric exchange of CO_2, CH_4 and N_2O in three subtropical forest ecosystems in southern China, Global Change Biol., 12, 546–560, 2006.

Tans, P. P., Fung, I. Y., and Takahashi, T.: Observation constraints on the global atmospheric CO_2 budget, Science, 247, 1431–1438, 1990.

Thompson, R. L., Manning, A. C., Gloor, E., Schultz, U., Seifert, T., Hänsel, F., Jordan, A., and Heimann, M.: In-situ measurements of oxygen, carbon monoxide and greenhouse gases from Ochsenkopf tall tower in Germany, Atmos. Meas. Tech., 2, 573–591, doi:10.5194/amt-2-573-2009, 2009.

Thoning, K. W., Tans, P. P., and Komhyr, W. D.: Atmoshperic carbon dioxide at Mauna Loa observatory 2. Analysis of the NOAA GMCC data, 1974–1985, J. Geophys. Res., 94, 8549–5865, 1989.

Wang, H., Zhou, L., and Tang, X.: Ozone concentrations in Rural Regions of the Yangtze Delta in China, J. Atmos. Chem., 54, 255–265, 2006.

WMO – World Meteorological Organization: WMO World Data Centre for Greenhouse Gases (WDCGG) Data Summary: Greenhouse Gases and Other Atmospheric Gases, No. 36, Japan Meteorological Agency, http://ds.data.jma.go.jp/gmd/wdcgg/products/summary/sum36/sum36contents.html (last access: 20 May 2013), 2012.

WMO Greenhouse Gas Bulletin: The state of greenhouse gases in the atmosphere based on global observations through 2010, World Meteorological Organization, Geneva, 2011.

WMO Greenhouse Gas Bulletin: The state of greenhouse gases in the atmosphere based on global observations through 2011, World Meteorological Organization, Geneva, 2012.

Xing, Y., Xie, P., Yang, H., Ni, L., Wang, Y., and Rong, K.: Methane and carbon dioxide fluxes from a shallow hypereutrophic subtropical lake in China, Atmos. Environ., 39, 5532–5540, 2005.

Yue, J., Shi, Y., Liang, W., Wu, J., Wang, C., and Huang, G.: Methane and nitrous oxide emissions from rice field and related microorganism in black soil, northeastern China, Nutr. Cycl. Agroecosys., 73, 293–301, 2005.

Zeng, N., Ding, Y., Pan, J., Wang, H., and Gregg, J.: Climate Change – the Chinese Challenge, Science, 319, 730–731, 2008.

Zhang, D., Tang, J., Shi, G., Nakazawa, T., Aoki, S., Sugawara, S., Wen, M., Morimoto, S., Patra, P. K., and Hayasaka, T.: Temporal and spatial variations of the atmospheric CO_2 concentration in China, Geophys. Res. Lett., 35, L03801, doi:10.1029/2007GL032531, 2008.

Zhao, C. L., Tans, P. P., and Thoning, K. W.: A high precision manometric system for absolute calibrations of CO_2 in dry air, J. Geophys. Res., 102, 5885–5894, 1997.

Zhao, C. L. and Tans, P. P.: Estimating uncertainty of the WMO mole fraction scale for carbon dioxide in air, J. Geophys. Res., 111, D08S09, doi:10.1029/2005JD006003, 2006.

Zhou, L., Tang, J., Wen, Y., Zhang, X., and Nie, H.: Impact of local surface wind on the atmospheric carbon dioxide background concentration at Mt. Waliguan, Acta Scient. Circumstant., 22, 135–139, 2002.

Zhou, L., Conway, T. J., White, J. W. C., Mukai, H., Zhang, X., Wen, Y., Li, J., and MacClune, K.: Long-term record of atmospheric CO_2 and stable isotopic ratios at Waliguan Observatory: Background features and possible drivers, 1991–2002, Global Biogeochem. Cy., 19, GB2001, doi:10.1029/2004GB002430, 2005.

Zhou, L. X., Tang, J., Wen, Y. P., Li, J. L., Yan, P., and Zhang, X. C.: The impact of local winds and long-range transport on the continuous carbon dioxide record at Mount Waliguan, China, Tellus B, 55, 145–158, 2003.

Zhou, L. X., Worthy, D. E. J., Lang, P. M., Ernst, M. K., Zhang, X. C., Wen, Y. P., and Li, J. L.: Ten years of atmospheric methane observations at a high elevation site in Western China, Atmos. Environ., 38, 7041–7054, 2004.

Zhou, L. X., White, J. W. C., Conway, T. J., Mukai, H., MacClune, K., Zhang, X., Wen, Y., and Li, J.: Long-term record of atmospheric CO_2 and stable isotopic ratios at Waliguan Observatory: Seasonally averaged 1991–2002 source/sink signals, and a comparison of 1998–2008 record to the 11 selected sites in the Northern Hemisphere, Global Biogeochem. Cy., 20, GB2001, doi:10.1029/2004GB002431, 2006.